

## Kerr dispersion in a Y-configuration quantum dot system

This content has been downloaded from IOPscience. Please scroll down to see the full text.

2014 J. Opt. 16 105205

(<http://iopscience.iop.org/2040-8986/16/10/105205>)

View [the table of contents for this issue](#), or go to the [journal homepage](#) for more

Download details:

IP Address: 161.139.19.2

This content was downloaded on 07/09/2014 at 12:02

Please note that [terms and conditions apply](#).

# Kerr dispersion in a Y-configuration quantum dot system

B Al-Nashy<sup>1,3</sup>, S M M Ameen<sup>1</sup> and Amin H Al-Khursan<sup>2</sup>

<sup>1</sup>Physics Dept., College of Science, University of Basrah, Basrah, Iraq

<sup>2</sup>Nassiriya Nanotechnology Research Laboratory (NNRL), Physics Dept., Science College, Thi-Qar University, Nassiriya, Iraq

<sup>3</sup>Science College, Missan University, Missan, Iraq

E-mail: [ameen\\_2all@yahoo.com](mailto:ameen_2all@yahoo.com)

Received 20 March 2014, revised 27 June 2014

Accepted for publication 25 July 2014

Published 4 September 2014

## Abstract

We introduce a Y-configuration model for a double quantum dot (QD) system, which is modeled for Kerr nonlinearity using the density matrix theory. Inhomogeneity in QDs is included in the calculations of the real part (Kerr) and the imaginary part (absorption) of the density matrix, which has not been covered before in Kerr calculations. Five configurations are studied: Y, ladder,  $\Lambda$ , staircase, and weak probe. Frequency detunings, controlling fields, and phases are used to study the structures. Our system shows high controllability as well as a giant Kerr dispersion, propagation without distortion, wide electromagnetic induced transparency, and switching between subluminal to superluminal propagation by tuning its fields.

Keywords: quantum dot, Kerr dispersion, absorption

(Some figures may appear in colour only in the online journal)

## 1. Introduction

Many quantum optical applications depend on Kerr nonlinearity, which is the real part of a third-order nonlinear susceptibility. For example, generation of optical solitons depends on cross-phase modulation, which can be enhanced with Kerr nonlinearity. Additionally, quantum information processing applications, such as Bell-state measurements, long-distance quantum teleportation and quantum bit generation are shown to be possible with giant Kerr nonlinearity [1–6]. When it is plotted against detuning, Kerr nonlinearity can be compared with linear absorption (the imaginary part of a first-order linear susceptibility). When absorption associates with Kerr dispersion in a medium it produces a wave distortion, while gain produces a noise that is accompanied by a wave travelling in the medium. Thus, a high Kerr nonlinearity dispersion at zero absorption (or zero gain) is preferred in order to transmit waves without distortion or noise. Much attention has been devoted to quantum dot (QD) structures due to their useful properties, especially discrete energy subbands and long dephasing time. These properties have gained QDs much attention in quantum optics applications and many studies have been devoted to them. For example,

She *et al* [7] studied the linear and nonlinear Kerr optical properties including interdot tunnel coupling and showed the possibility of their modulation by the control field. Mahmoudi *et al* [8] controlled the switching of group velocity in QDs by tunneling. Hao *et al* discussed the case of manipulation between pump and coupling fields and showed their effect on linear dispersion and four-wave mixing in a four-level QD structure [9]. In conclusion, much work has been done that includes tunneling between double QDs and four-level single QD systems. Hamedi *et al* [10] obtained high gain and dispersion in an atomic Y-structure. Joshi [11] examined the inverted Y-structure in quantum well structures and showed the possibility of a single parameter control. In nano-systems, the Y-structure offers the possibility of intersubband transitions [11]. Due to QD subband quantization, it is easy to realize the Y-scheme using its conduction intersubband transitions.

No previous work has studied Y-structure in QDs. This work proposes a four-level double QD Y-structure as an appropriate system for high Kerr dispersion at low absorption. An analytical relation is obtained from the density matrix equations, which is then simulated by MATLAB. The results discuss the possibilities of this system by turning off one of

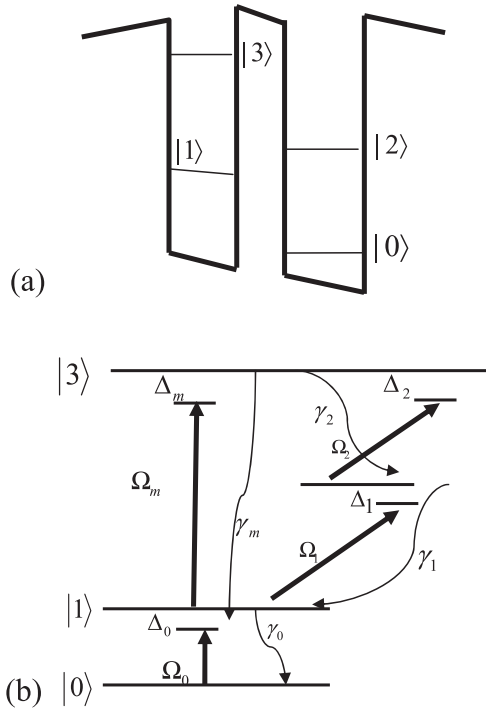


**Figure 1.** Schematic energy level diagram of a four-level system in Y-configuration. Here,  $\omega_0(\Delta_0)$ ,  $\omega_1(\Delta_1)$ ,  $\omega_2(\Delta_2)$ , and  $\omega_m(\Delta_m)$  are frequencies (frequency detunings) of probe, cycling, coupling, and pumping fields, respectively.

the four applied fields which results in new schemes such as the  $\Lambda$ -, staircase- and ladder-scheme, while the other two cases remain Y-scheme. In [11] and [10], the pump and probe field couples with the two-photon process via two pumping fields (pump and coupling fields). This makes it possible to strengthen the Kerr peak by manipulating these two fields, which are not offered by the atomic Y-structures.

In this work, interesting possibilities are explored, wherein the structure returns to a simple two-level system in many of the discussed cases. The benefit of our structure here is a high Kerr value that cannot be obtained with any other real, simple two-level system. This results from the collective work of the four fields. It is shown that the cycling field produces the strength of the Kerr dispersion. Additionally, due to their manufacture imperfections, the QDs have a nonuniformity in shape and size distribution [12]. Inclusion of inhomogeneous broadening is shown in order to best demonstrate the experimental results of gain and refractive index [13]. This work will show that inhomogeneity, which has not yet been considered in the literature on Kerr calculation, drastically reduces QDs Kerr nonlinearity in a non-neglected range.

## 2. Y-type model in double QD nanostructures

Consider a four-level Y-type configuration in a QD system. This can be found in a QD molecule, as in figure 1, which depicts a double QD with two conduction band levels apiece. The intersubband transitions are easily done experimentally. The subbands' configuration has two subsystems. Subbands

$|0\rangle, |1\rangle, |2\rangle$  and  $|3\rangle$  form a  $\Lambda$ -type system with the  $|0\rangle \rightarrow |1\rangle$  transition ( $\hbar\omega_{10}$  energy) due to the weak probe field  $E_0$ , (frequency  $\omega_0$ ) with Rabi frequency ( $\Omega_0 = E_0\mu_{10}/2\hbar$ ; note that  $\mu_{10}$  is the dipole moment of this transition); the  $|1\rangle \rightarrow |2\rangle$  transition ( $\hbar\omega_{21}$  energy) due to the strong cycling field  $E_1$ , (frequency  $\omega_1$ ) with Rabi frequency ( $\Omega_1 = E_1\mu_{21}/2\hbar$ ); and the  $|2\rangle \rightarrow |3\rangle$  transition ( $\hbar\omega_{32}$  energy) due to the coupling field  $E_2$ , (frequency  $\omega_2$ ) with Rabi frequency ( $\Omega_2 = E_2\mu_{32}/2\hbar$ ). The second subsystem contains  $|0\rangle, |1\rangle$  and  $|3\rangle$  subbands and forms a ladder-type system with the  $|0\rangle \rightarrow |1\rangle$  transition and the  $|1\rangle \rightarrow |3\rangle$  transition ( $\hbar\omega_{13}$  energy) due to the strong pump field  $E_3$ . The corresponding detunings for these transitions are  $\Delta_2 = \omega_2 - \omega_{23}$ ,  $\Delta_m = \omega_m - \omega_{13}$ ,  $\Delta_1 = \omega_1 - \omega_{12}$ , and  $\Delta_0 = \omega_0 - \omega_{01}$ , respectively. In this way, the two middle levels  $|1\rangle$  and  $|2\rangle$ , the upper level  $|3\rangle$ , and the ground level  $|0\rangle$  form a closed interaction contour. The phases associated with the four coherent fields  $E_0, E_1, E_2$ , and  $E_m$  are  $\phi_0, \phi_1, \phi_2$ , and  $\phi_m$ , respectively.

Using the density matrix approach for our system, shown in figure 1, and under the rotating-wave and electric-dipole approximations, the time evolution of the system, expressed by the density operator  $\rho$ , leads to the following system of equations for the density matrix elements  $\rho_{ij}$ :

$$\begin{aligned} \rho_{00}^{(3)} &= -\gamma_0\rho_{00}^{(3)} + i\Omega_0(\rho_{10}^{(2)} - \rho_{01}^{(2)}) \\ \rho_{11}^{(3)} &= -(\gamma_0\rho_{11}^{(3)} + \gamma_1\rho_{22}^{(3)} + \gamma_3\rho_{33}^{(3)}) \\ &\quad + i[\Omega_0(\rho_{01}^{(2)} - \rho_{10}^{(2)}) \\ &\quad + \Omega_2(\rho_{21}^{(2)} - \rho_{12}^{(2)})\Omega_m(\rho_{31}^{(2)} - \rho_{13}^{(2)})] \\ \rho_{22}^{(3)} &= -(\gamma_1\rho_{22}^{(3)} + \gamma_2\rho_{33}^{(3)}) \\ &\quad + i[\Omega_1(\rho_{12}^{(2)} - \rho_{21}^{(2)}) \\ &\quad + \Omega_2(\rho_{32}^{(2)} - \rho_{23}^{(2)})] \\ \rho_{33}^{(3)} &= -(\gamma_2 + \gamma_3)\rho_{33}^{(3)} \\ &\quad + i[\Omega_m(\rho_{13}^{(2)} - \rho_{31}^{(2)}) \\ &\quad + \Omega_2(\rho_{23}^{(2)} - \rho_{32}^{(2)})] \\ \rho_{10}^{(3)} &= -(i\Delta_0 + \gamma_0)\rho_{10}^{(3)} \\ &\quad + i[\Omega_0(\rho_{00}^{(2)} - \rho_{11}^{(2)}) \\ &\quad + \Omega_1\rho_{20}^{(2)}e^{i\phi} + \Omega_m\rho_{30}^{(2)}] \\ \rho_{20}^{(3)} &= [-i(\Delta_0 + \Delta_1) - (\gamma_0 + \gamma_1)]\rho_{20}^{(3)} \\ &\quad + i[\Omega_1\rho_{10}^{(2)}e^{i\phi} + \Omega_2\rho_{30}^{(2)} - \Omega_0\rho_{21}^{(3)}e^{i\phi}] \\ &\quad + i[\Omega_1\rho_{10}^{(2)}e^{i\phi} + \Omega_2\rho_{30}^{(2)} - \Omega_0\rho_{21}^{(3)}e^{i\phi}] \\ \rho_{30}^{(3)} &= [-i(\Delta_0 + \Delta_m + \Delta_2) - (\gamma_0 + \gamma_2 + \gamma_3)]\rho_{30}^{(3)} \\ &\quad + i[\Omega_m\rho_{10}^{(2)} + \Omega_2\rho_{20}^{(2)} - \Omega_0\rho_{31}^{(2)}] \end{aligned}$$

$$\begin{aligned}
 \rho_{12}^{(3)} &= -[i\Delta_0 + i\Delta_1 + \gamma_1]\rho_{12}^{(3)} \\
 &+ i\left[\Omega_0\rho_{02}^{(2)}e^{i\varphi} + \Omega_1(\rho_{22}^{(2)} - \rho_{11}^{(2)})\right. \\
 &+ \left.\Omega_m\rho_{32}^{(2)}e^{i\varphi} - \Omega_2\rho_{13}^{(2)}e^{i\varphi}\right] \\
 \rho_{13}^{(3)} &= -(i\Delta_m + i\Delta_2 + \gamma_2 + \gamma_3)\rho_{13}^{(3)} \\
 &+ i\left[\Omega_m(\rho_{33}^{(2)} - \rho_{11}^{(2)}) + \Omega_0\rho_{03}^{(2)}\right. \\
 &+ \left.\Omega_1\rho_{23}^{(2)} - \Omega_2\rho_{12}^{(2)}e^{i\varphi}\right] \\
 \rho_{23}^{(3)} &= \left[-i(\Delta_0 + \Delta_m + \Delta_2) - (\gamma_2 + \gamma_3)\right]\rho_{23}^{(3)} \\
 &+ i\left[\Omega_2(\rho_{33}^{(2)} - \rho_{22}^{(2)}) + \Omega_1\rho_{13}^{(2)} - \Omega_m\rho_{21}^{(2)}e^{i\varphi}\right] \quad (1)
 \end{aligned}$$

Note that  $\gamma_i$  is the total decay rate from subband (i) and includes both the lifetime broadening due to longitudinal phonon emission at low temperature and the dephasing broadening, which results from both acoustic phonon scattering and scattering from interface roughness. In QDs, dephasing broadening is the dominant contribution, in contrast to the atomic systems [9].

The third-order nonlinear Kerr effect is calculated from the probe transition coherence  $\rho_{10}^{(3)}$ . An analytical relationship can be obtained by taking the solution of the system equations (1) at steady state. After some (long) mathematical manipulations, one can get the following relationship:

$$\begin{aligned}
 \rho_{10}^{(3)} &= \left\{ \frac{-\Omega_0^2}{\gamma_0} \left[ -i\Omega_0 + \frac{\Omega_0\Omega_1\rho_{21}e^{2i\varphi}}{a} \right. \right. \\
 &+ \left. \left. \frac{-\Omega_2\Omega_m\rho_{20}}{-b} \right] \left[ (i\Delta_0 + \gamma_0) + \frac{\Omega_1^2 e^{2i\varphi}}{a} + \frac{\Omega_m^2}{b} \right]^{-1} \right. \\
 &+ \frac{\Omega_0^2}{\gamma_0} \left[ i\Omega_0 + \frac{-\Omega_0\Omega_1\rho_{21}e^{-2i\varphi}}{a} \right. \\
 &+ \left. \frac{\Omega_2\Omega_m\rho_{20}}{b} \right] \left[ (i\Delta_0 + \gamma_0) - \frac{\Omega_1^2 e^{-2i\varphi}}{a} - \frac{\Omega_m^2}{b} \right]^{-1} \\
 &+ \frac{-\Omega_1\Omega_0e^{2i\varphi}}{a} \left[ -i\Omega_0 + \frac{\Omega_0\Omega_1\rho_{21}e^{2i\varphi}}{a} \right. \\
 &+ \left. \frac{-\Omega_2\Omega_m\rho_{20}}{b} \right] \left[ (i\Delta_0 + \gamma_0) + \frac{\Omega_1^2 e^{2i\varphi}}{a} + \frac{\Omega_m^2}{b} \right]^{-1} \\
 &+ \frac{-\Omega_2\Omega_1e^{i\varphi}}{a} \left[ \frac{i(\Omega_m\rho_{10} + \Omega_2\rho_{20})}{b} \right] \\
 &+ \frac{\Omega_0\Omega_1e^{2i\varphi}}{a} \left[ \frac{-i(\Omega_0\rho_{20}e^{-i\varphi} - \Omega_1)}{[-i\Delta_1 + (\gamma_1 + \gamma_0)]} \right] \\
 &+ \left. \frac{-\Omega_m^2}{b} \left[ -i\Omega_0 + \frac{\Omega_0\Omega_1\rho_{21}e^{2i\varphi}}{a} \right] \right\}
 \end{aligned}$$

$$\begin{aligned}
 &+ \frac{-\Omega_2\Omega_m\rho_{20}}{b} \left] \left[ (i\Delta_0 + \gamma_0) + \frac{\Omega_1^2 e^{2i\varphi}}{a} + \frac{\Omega_m^2}{b} \right]^{-1} \right. \\
 &+ \left. \frac{i(\Omega_2\Omega_m\Omega_1\rho_{10}e^{i\varphi} - \Omega_2\Omega_m\Omega_0\rho_{21}e^{i\varphi})}{b \cdot a} \right. \\
 &+ \left. \frac{i(\Omega_0\Omega_m^2 + \Omega_0\Omega_m\Omega_2\rho_{21}e^{i\varphi})}{b \cdot [-i(\Delta_m + \Delta_2) + \gamma_2 + \gamma_3]} \right] \left[ \frac{1}{(i\Delta_0 + \gamma_0)} \right] \quad (2)
 \end{aligned}$$

where  $a = i(\Delta_0 + \Delta_1) + (\gamma_0 + \gamma_1)$ ,  $b = i(\Delta_0 + \Delta_m + \Delta_2) + (\gamma_0 + \gamma_2 + \gamma_3)$ , and  $\phi = \phi_0 + \phi_2 - \phi_1$ . The nonlinear Kerr susceptibility is then given by

$$\chi^{(3)}(\omega_0) = \int \frac{2N\mu_{01}^4}{3\hbar^3\epsilon_0\Omega_0^3}\rho_{01}^{(3)}(\omega_0)D(\omega)d\omega, \quad (3)$$

where  $N$  is the atomic number density in the medium. Our formula differs from all previous calculations because of convolution the inhomogeneous density of states in QDs is then given by [14]:

$$D(E) = \frac{s^i}{V_{dot}^{eff}} \frac{1}{\sqrt{2\pi\sigma^2}} \exp\left(\frac{-(\hbar\omega - E_{max}^i)^2}{2\sigma^2}\right), \quad (4)$$

where  $s^i$  is the degeneracy number at QD state, ( $s^i = 2$ ) in the quantum disc model used here,  $\sigma$  is the spectral variance of QDs,  $V_{dot}^{eff} (= h/N_D)$  is the effective volume of QDs,  $h$  is the dot height and  $N_D$  is the areal density of QDs. The transition energy at the QD maximum distribution of the  $i$ th optical transition is  $E_{max}^i$ .

### 3. The proposed QD structure

The proposed structure used to simulate the system shown in figure 1 is an asymmetric InAs double QDs with 10 nm height and 4 nm width for the left dot, and 14 nm height and 2 nm width for the right dot. Their ground and excited conduction energy subbands are (0.8 and 1.07 eV) for the left QD and (0.91 and 1.05 eV) for the right. This structure can be obtained by the self-assemble growth technique [15]. The ground state (GS) for the left dot is the state  $|0\rangle$  of the system, while the GS and ES of the right dot are the states  $|1\rangle$  and  $|2\rangle$ , and the state  $|3\rangle$  is the ES of the left dot. Inclusion of inhomogeneity, as mentioned above, is important for susceptibility calculations. This has not previously been discussed in the QD literature on quantum coherence and interference; see for example [2, 7, 16–19]. Results are divided into subsections.

### 4. Special cases for Y-configuration QD structures

Examining equation (2), there are many cases for our structure that can be discussed. Below, the obtained relation of each case with its results are shown and discussed in their respective subsections. For all of the figures below, the Kerr dispersion,

which is the real part of third-order nonlinear susceptibility, is shown as a red solid line; the nonlinear absorption (or gain), which is the imaginary part of the third-order susceptibility, is shown as a red dashed line; and the linear absorption (gain), which is the imaginary part of linear susceptibility, is shown as a blue dashed line. All the relaxations are assumed to be equal, i.e. ( $\gamma_0 = \gamma_1 = \gamma_2 = \gamma_3 = \gamma = 1$  meV). Assumption of identical relaxation is used for simplifying the calculations and can be found in [17] for a QD system, in [1] for an atomic system, and in [11] for a quantum well system. Before going into a discussion of the case, let us study the structure where all fields are turned on. This is the case where equation (2) is used. The nonlinear susceptibility spectrum from equation (2) is plotted in figure 2 versus the probe detuning ( $\Delta_0$ ), which is normalized by its relaxation rate ( $\gamma_0$ ). The parameters used are for the Rabi frequencies  $\Omega_0 = 0.01\gamma$ ,  $\Omega_1 = 0.1\gamma$ ,  $\Omega_2 = 0.1\gamma$ ,  $\Omega_m = 1\gamma$ , while the detunings are ( $\Delta_1 = \Delta_2 = 5\gamma$ ,  $\Delta_m = 3\gamma$ ). A positive Kerr peak near zero probe detuning is shown. A two-sided Kerr peak appears at different distances from the central peak. This may result from the different field detunings ( $\Delta_1$ ,  $\Delta_2$ ,  $\Delta_m$ ). For the linear absorption (multiplied by a factor of 50, for figure clarity) an electromagnetic induced transparency (EIT) window is shown. The curve of the Kerr dispersion, assuming homogeneous broadening, is shown as a solid black curve. An inhomogeneously broadening curve lowers the homogeneously broadening one by a factor of four, due to size and shape fluctuations [20]. Thus, it is critical to include inhomogeneity in the Kerr calculations of QD structures. In the following results, inhomogeneity is included.

The discussed cases are:

a. Y-configuration for  $E_2 = 0$  case

Dropping the coupling field, the two dots are still connected by the probe field. Equation (2) for this case, becomes

$$\begin{aligned} \rho_{10}^{(3)} = & \left\{ \frac{-\Omega_0^2}{\gamma_0} \left[ -i\Omega_0 + \frac{\Omega_0\Omega_1\rho_{21}e^{2i\phi}}{a} \right] \right. \\ & \times \left[ (i\Delta_0 + \gamma_0) + \frac{\Omega_1^2 e^{2i\phi}}{a} + \frac{\Omega_m^2}{b} \right]^{-1} \\ & + \frac{\Omega_0^2}{\gamma_0} \left[ i\Omega_0 - \frac{\Omega_0\Omega_1\rho_{21}e^{-2i\phi}}{a} \right] \\ & \times \left[ (i\Delta_0 + \gamma_0) - \frac{\Omega_1^2 e^{-2i\phi}}{a} - \frac{\Omega_m^2}{b} \right]^{-1} \\ & - \frac{\Omega_1\Omega_0 e^{2i\phi}}{a} \left[ \frac{\Omega_0\Omega_1\rho_{21}e^{2i\phi}}{a} - i\Omega_0 \right] \\ & \times \left[ (i\Delta_0 + \gamma_0) + \frac{\Omega_1^2 e^{2i\phi}}{a} + \frac{\Omega_m^2}{b} \right]^{-1} \\ & - \frac{\Omega_0\Omega_1 e^{2i\phi}}{a} \left[ \frac{i(\Omega_0\rho_{20}e^{-i\phi} - \Omega_1)}{[-i\Delta_1 + (\gamma_1 + \gamma_0)]} \right] \end{aligned}$$

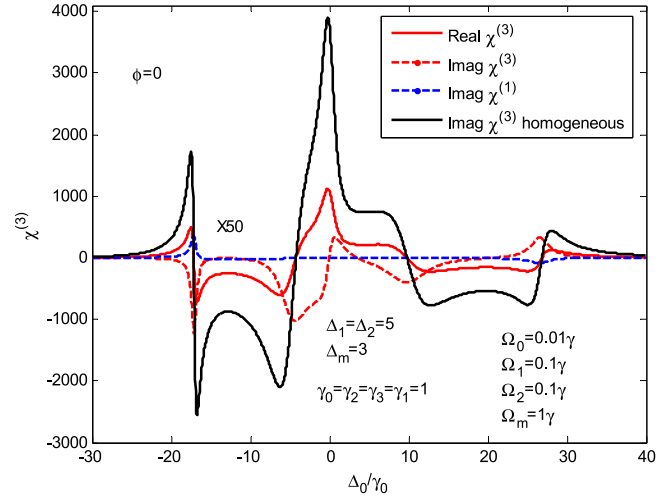


**Figure 2.** Third-order susceptibility as a function of probe detuning, ( $\Delta_0$ ), normalized to the decay rate ( $\gamma_0$ ) when  $\Omega_0 = 0.01\gamma$ ,  $\Omega_1 = 0.1\gamma$ ,  $\Omega_2 = 0.1\gamma$ ,  $\Omega_m = 1\gamma$ , ( $\Delta_1 = \Delta_2 = 5\gamma$ ,  $\Delta_m = 3\gamma$ ). Note that ( $\gamma_0 = \gamma_1 = \gamma_2 = \gamma_3 = \gamma = 1$  meV).

$$\begin{aligned} & + \frac{i(\Omega_0\Omega_m^2)}{b[-i(\Delta_m + \Delta_2) + \gamma_2 + \gamma_3]} \left] - \frac{\Omega_m^2}{b} \right. \\ & \times \left[ -\Omega_0 + \frac{\Omega_0\Omega_1\rho_{21}e^{2i\phi}}{a} \right] \left[ (i\Delta_0 + \gamma_0) + \frac{\Omega_1^2 e^{2i\phi}}{a} \right. \\ & \left. \left. + \frac{\Omega_m^2}{b} \right]^{-1} \right] \cdot \left[ \frac{1}{(i\Delta_0 + \gamma_0)} \right] \end{aligned} \quad (5)$$

For the special Y-case, equation (5), figure 3(a) shows the absorption and dispersion spectra when the coupling field is turned off. The structure works at the detunings  $\Delta_1 = 3\gamma$ ,  $\Delta_2 = \Delta_m = 0$ , while the Rabi frequency of the pump increases to  $\Omega_m = 0.5\gamma$ . A negative slope for Kerr dispersion is shown around zero probe detuning, which indicates superluminal propagation. It also occurs at neglected absorption, which indicates propagation without distortion (the absorption curve in the figure is multiplied by 70 for clarity). The case of superluminal propagation is required to achieve the theoretical limit of information transmission since some transmission systems are not optimal. It is also important when the measurements of information content must be performed near the peak pulse where the wave propagates at or below the speed of light in a vacuum [8]. The figure also refers to the possibility of switching from subluminal to superluminal light propagation. The reduction in the Kerr height here results from reducing the pump field to  $\Omega_m = 0.5\gamma$ . Figure 3(b) shows the case when  $\Delta_1 = \Delta_m = 0$ ,  $\Delta_2 = 3\gamma$ . A steep curve around zero probe detuning is shown which refers to a huge Kerr dispersion. It occurs at neglected absorption (recall that the absorption curve is multiplied by 70). This figure shows the importance of the coupling field. The structure returns to a simple two-level system when  $E_2 = 0$  since each dot behaves separately in the presence of a weak probe field, where both cycling and pump fields are in resonance with their transitions. Then an

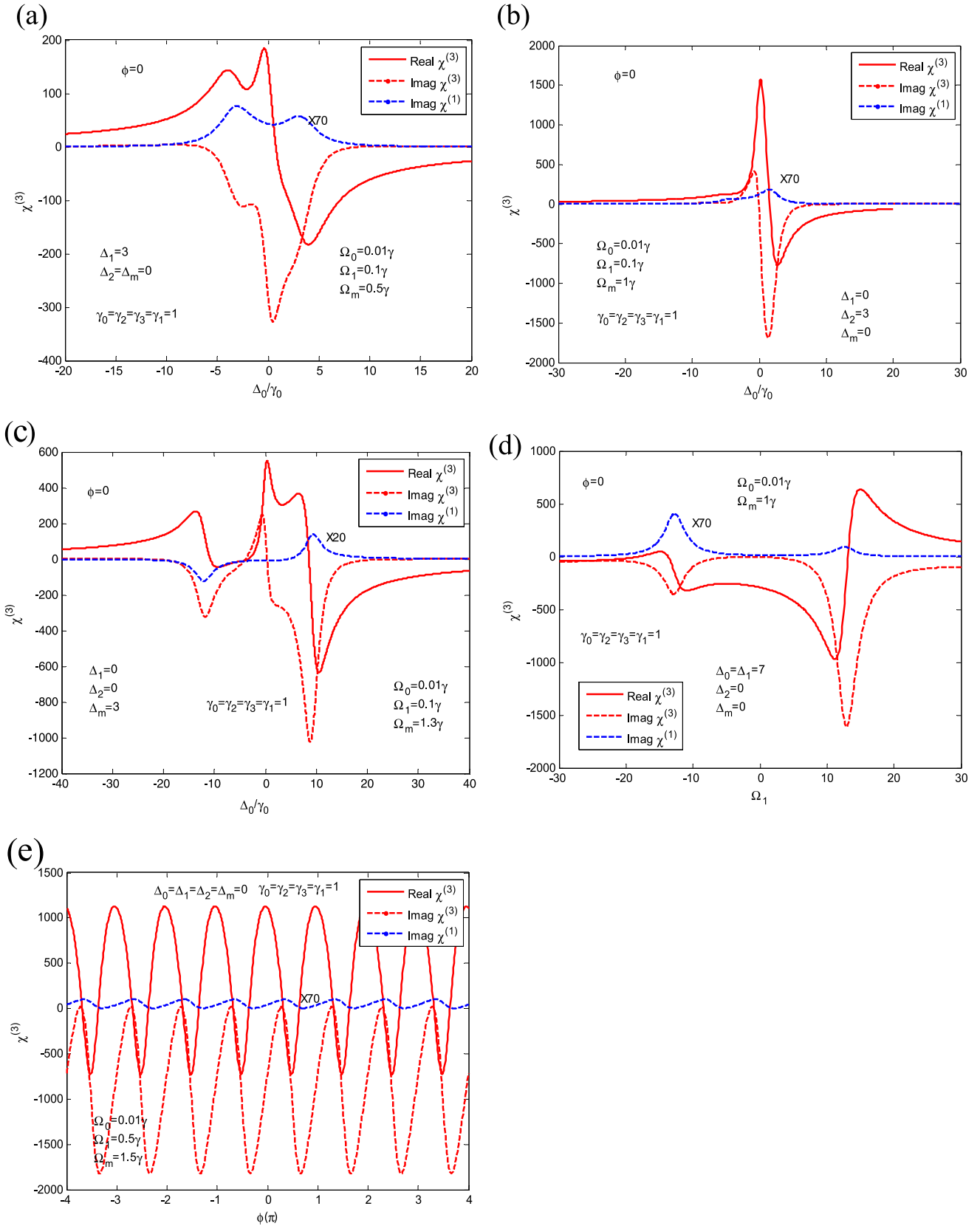


**Figure 3.** Third-order susceptibility for Y-case ( $E_0=0$ ) in (a), (b) and (c) as a function of probe detuning, with ( $\Delta_0$ ) normalized to the decay rate ( $\gamma_0$ ). Note that in (a)  $\Omega_0 = 0.01\gamma$ ,  $\Omega_1 = 0.1\gamma$ ,  $\Omega_m = 0.5\gamma$ , ( $\Delta_1 = 3\gamma$ ,  $\Delta_2 = \Delta_m = 0$ ); in (b) ( $\Omega_0 = 0.01\gamma$ ,  $\Omega_1 = 0.1\gamma$ ,  $\Omega_m = \gamma$ ) ( $\Delta_1 = 0$ ,  $\Delta_2 = 3\gamma$ ,  $\Delta_m = 0$ ); in (c) ( $\Omega_0 = 0.01\gamma$ ,  $\Omega_1 = 0.1\gamma$ ,  $\Omega_m = 1.3\gamma$ ), ( $\Delta_1 = \Delta_2 = 0$ ,  $\Delta_m = 3\gamma$ ); in (d) as a function of cycling field Rabi energy  $\Omega_1$  when ( $\Omega_0 = 0.01\gamma$ ,  $\Omega_m = \gamma$ ), ( $\Delta_0 = \Delta_1 = 7\gamma$ ,  $\Delta_2 = \Delta_m = 0$ ); and in (e) as a function of phase. Note that ( $\gamma_0 = \gamma_1 = \gamma_2 = \gamma_3 = \gamma = 1$  meV).

absorption peak replaces the EIT window. Figure 3(c) shows the nonlinear susceptibility when the pump is detuned to  $\Delta_m = 3\gamma$  while  $\Delta_1 = \Delta_2 = 0$ . A positive and steep Kerr dispersion is obtained near zero probe detuning. A wide EIT window is obtained which is half that of the window in figure 2, since the structure is still a four-level Y-structure. A Kerr peak near zero detuning is obtained at zero absorption, which is preferred for use in most applications. Figures 3(a)–(c) show the controllability of our structure by a single parameter, the detuning. Figure 3(d) shows the nonlinear susceptibility as a function of Rabi cycling ( $\Omega_1$ ), which is an example of field detuning. A high, positive Kerr dispersion is obtained when the cycling field approaches ( $15\gamma$ ) with a zero absorption (which is multiplied by 70, for figure clarity) at this region. The figure also shows the possibility of switching between superluminal and subluminal light propagation via the cycling field. Figure 3(e) shows the nonlinear susceptibility as a function of phase. The zero absorption is shown (which is also multiplied by 70, for figure clarity). Kerr dispersion is periodically phase dependent on the  $\pi$ -period.

b. For  $E_1 = E_2 = 0$  ladder configuration

$$\rho_{10}^{(3)} = \left\{ \frac{-\Omega_0^2}{\gamma_0} [-i\Omega_0] \left[ (i\Delta_0 + \gamma_0) + \frac{\Omega_m^2}{b} \right]^{-1} + \frac{\Omega_0^2}{\gamma_0} [i\Omega_0] \left[ (i\Delta_0 + \gamma_0) - \frac{\Omega_m^2}{b} \right]^{-1} + \frac{-\Omega_m^2}{b} [-i\Omega_0] \left[ (i\Delta_0 + \gamma_0) + \frac{\Omega_m^2}{b} \right]^{-1} + \frac{-i(-\Omega_0\Omega_m^2)}{b \cdot [-i(\Delta_m + \Delta_2) + \gamma_2 + \gamma_3]} \right\} \left[ \frac{1}{(i\Delta_0 + \gamma_0)} \right] \quad (6)$$

For the ladder case, ( $E_1 = E_2 = 0$ ), figure 4(a) shows the absorption and dispersion spectra as a function of probe detuning; the detuning parameters are  $\Delta_1 = \Delta_m = 0$ ,  $\Delta_2 = 5\gamma$  and the Rabi field energies are  $\Omega_0 = 0.01\gamma$ ,  $\Omega_m = 1\gamma$ . Since the probe field is weak, the pump field is the only coupling between the two dots, and no EIT window, which would be a result of destructive interference between the pump and probe [21], is shown. Since the transition ( $|2\rangle \rightarrow |1\rangle$ ) is an allowed transition, there are two transitions at the same time: downward ( $|2\rangle \rightarrow |1\rangle$ ) and upward ( $|1\rangle \rightarrow |3\rangle$ ) under the effect of pump field. Finally, we are in a simple two-level configuration (simple  $|0\rangle \rightarrow |1\rangle$  system). A steep Kerr dispersion with positive slope near zero detuning is thus obtained, compared with figure 3(b) (which is also a two-level system), where Kerr height is reduced when the cycling field is canceled. This explains the higher Kerr dispersion obtained using the Y-configuration in figures 2 and 3, which are higher than all other Kerr values obtained by other systems previously reported in the literature. This results from the collective work of the four fields (three fields in figure 3). Here, the strength of the Kerr dispersion comes from the cycling field. Figure 4(b) shows the possibility of obtaining an EIT window when the Rabi energy of the pump is increased to

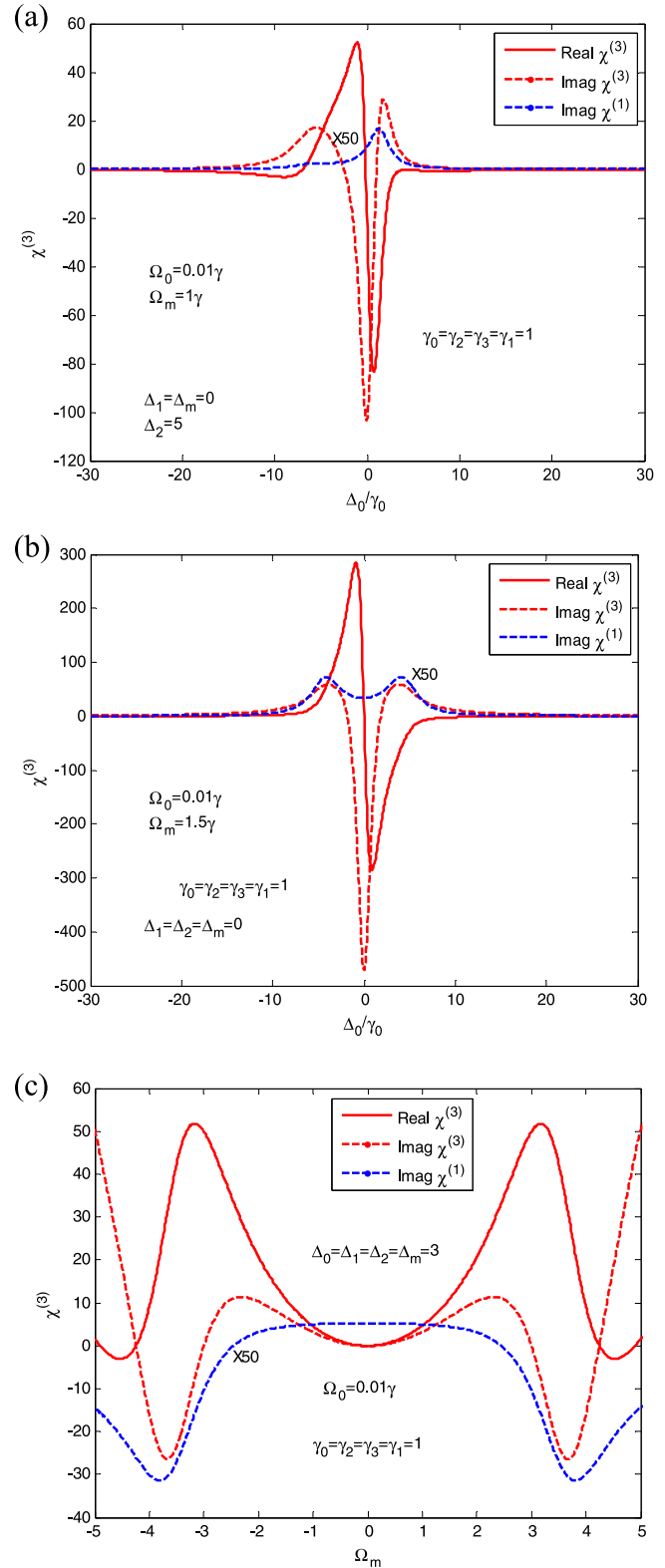


**Figure 4.** Third-order susceptibility for ladder configuration as a function of (a) and (b) probe detuning, ( $\Delta_0$ ), normalized to the decay rate ( $\gamma_0$ ), (a) when ( $\Omega_0 = 0.01\gamma$ ,  $\Omega_m = 1\gamma$ ), ( $\Delta_1 = \Delta_m = 0$ ,  $\Delta_2 = 5\gamma$ ); (b) when ( $\Omega_0 = 0.01\gamma$ ,  $\Omega_m = 1.5\gamma$ ); (c) as function of pump field Rabi energy  $\Omega_m$  when ( $\Omega_0 = 0.01\gamma$ ), ( $\Delta_0 = \Delta_1 = \Delta_2 = \Delta_m = 3\gamma$ ). Note that ( $\gamma_0 = \gamma_1 = \gamma_2 = \gamma_3 = \gamma = 1$  meV).

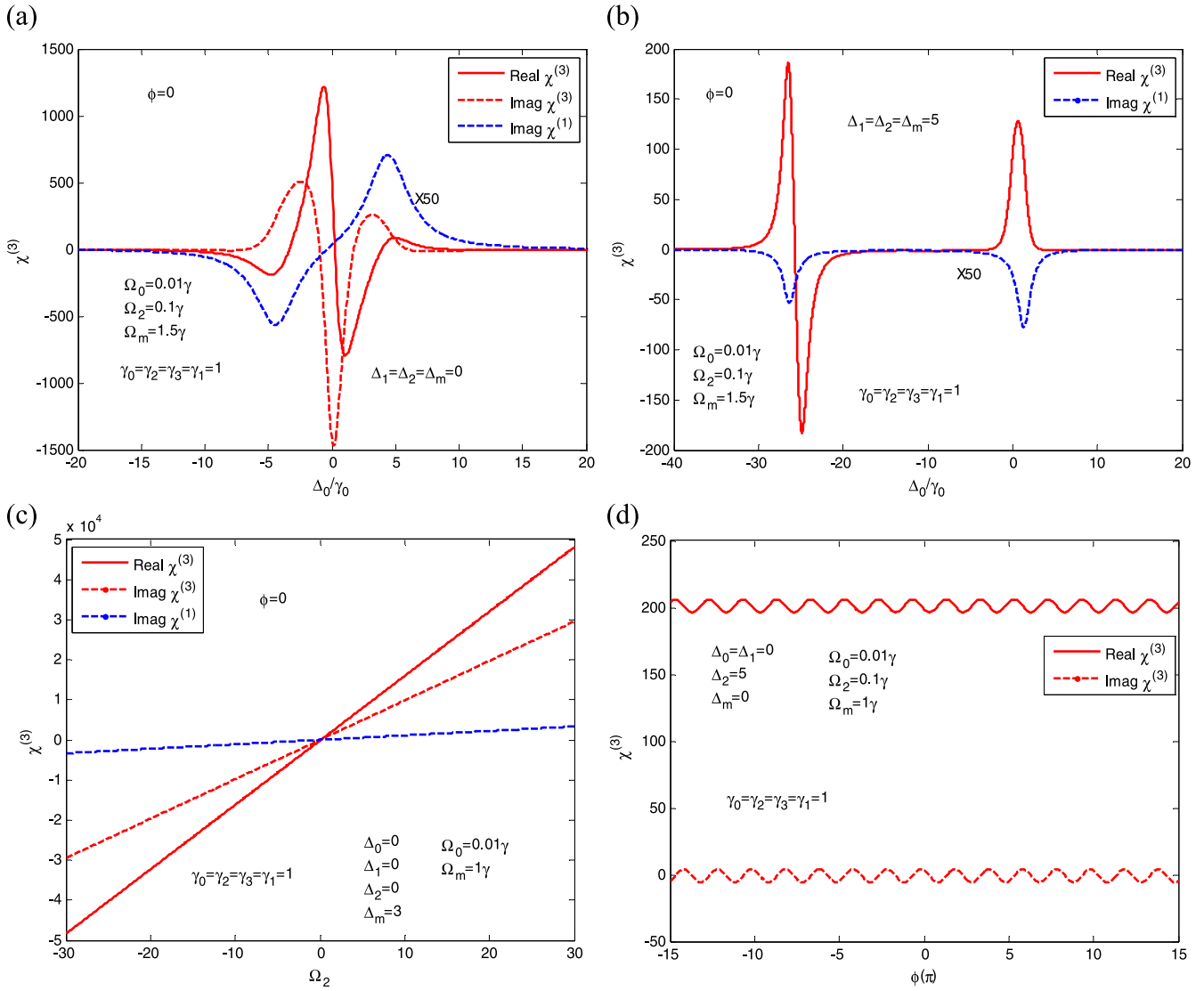


**Figure 5.** Third-order susceptibility for  $\Lambda$  configuration ( $E_1 = 0$ ) when (a) ( $\Omega_0 = 0.01\gamma$ ,  $\Omega_2 = 0.1\gamma$ ,  $\Omega_m = 1.5\gamma$ ), ( $\Delta_1 = \Delta_2 = \Delta_m = 0$ ); (b) ( $\Omega_0 = 0.01\gamma$ ,  $\Omega_2 = 0.1\gamma$ ,  $\Omega_m = 1.5\gamma$ ) and ( $\Delta_1 = \Delta_2 = \Delta_m = 5\gamma$ ) as a function of probe detuning, ( $\Delta_0$ ), normalized to the decay rate ( $\gamma_0$ ); (c) as function of coupling field Rabi energy  $\Omega_2$  when ( $\Omega_0 = 0.01\gamma$ ,  $\Omega_m = 1\gamma$ ) ( $\Delta_0 = \Delta_1 = \Delta_2 = 0$ ,  $\Delta_m = 3\gamma$ ); (d) as a function of phase when ( $\Omega_0 = 0.01\gamma$ ,  $\Omega_2 = 0.1\gamma$ ,  $\Omega_m = \gamma$ ). ( $\Delta_0 = \Delta_1 = 0$ ,  $\Delta_2 = 5\gamma$ ,  $\Delta_m = 0$ ). Note that ( $\gamma_0 = \gamma_1 = \gamma_2 = \gamma_3 = \gamma = 1$  meV).

( $\Omega_m = 1.5\gamma$ ) while all detunings are zero. Figure 4(c) shows that the control by the pumping field where Kerr dispersion peaks are obtained at ( $\Omega_m = \pm 3\gamma$ ) corresponds to a considerable linear gain, which results in unrequired noise associated with wave propagation. Due to this phenomenon, this case is not recommended for use in applications.

c. For  $E_1 = 0$ ,  $\Lambda$  configuration

$$\rho_{10}^{(3)} = \left[ \frac{1}{(i\Delta_0 + \gamma_0)} \right] \left\{ \left[ \frac{-\Omega_0^2}{\gamma_0} \left[ -i\Omega_0 + \frac{\Omega_2\Omega_m\rho_{20}}{b} \right] \right. \right. \\ \times \left[ \left( i\Delta_0 + \gamma_0 \right) + \frac{\Omega_m^2}{b} \right]^{-1} + \frac{\Omega_0^2}{\gamma_0} \left[ i\Omega_0 + \frac{\Omega_2\Omega_m\rho_{20}}{b} \right] \\ \left. \left. \times \left[ \left( i\Delta_0 + \gamma_0 \right) - \frac{\Omega_m^2}{b} \right]^{-1} + \frac{-\Omega_m^2}{b} \left[ -i\Omega_0 + \frac{-\Omega_2\Omega_m\rho_{20}}{b} \right] \right\}$$

$$\times \left[ \left( i\Delta_0 + \gamma_0 \right) + \frac{\Omega_m^2}{b} \right]^{-1} + \frac{i(\Omega_2\Omega_m\Omega_0\rho_{21}e^{i\phi})}{b \cdot a} \\ + \frac{i(\Omega_0\Omega_m^2 + \Omega_0\Omega_m\Omega_2\rho_{21}e^{i\phi})}{b \cdot \left[ -i(\Delta_m + \Delta_2) + \gamma_2 + \gamma_3 \right]} \quad (7)$$

For  $\Lambda$  configuration, ( $E_1 = 0$ ), figure 5(a) shows the linear and nonlinear absorption and Kerr dispersion spectra when the cycling field is turned off. EIT windows are obtained due to the four-level  $\Lambda$  configuration constructed from subband transitions ( $|0\rangle \rightarrow |1\rangle$ ,  $|1\rangle \rightarrow |3\rangle$ , and  $|2\rangle \rightarrow |3\rangle$ ). A steep and negative slope dispersion is shown around zero detuning which indicates superluminal light propagation. In figure 5(b), by controlling the detunings to  $\Delta_1 = \Delta_2 = \Delta_m = 5\gamma$ , a wide EIT window with reduced Kerr dispersion is obtained. Corresponding to these wide

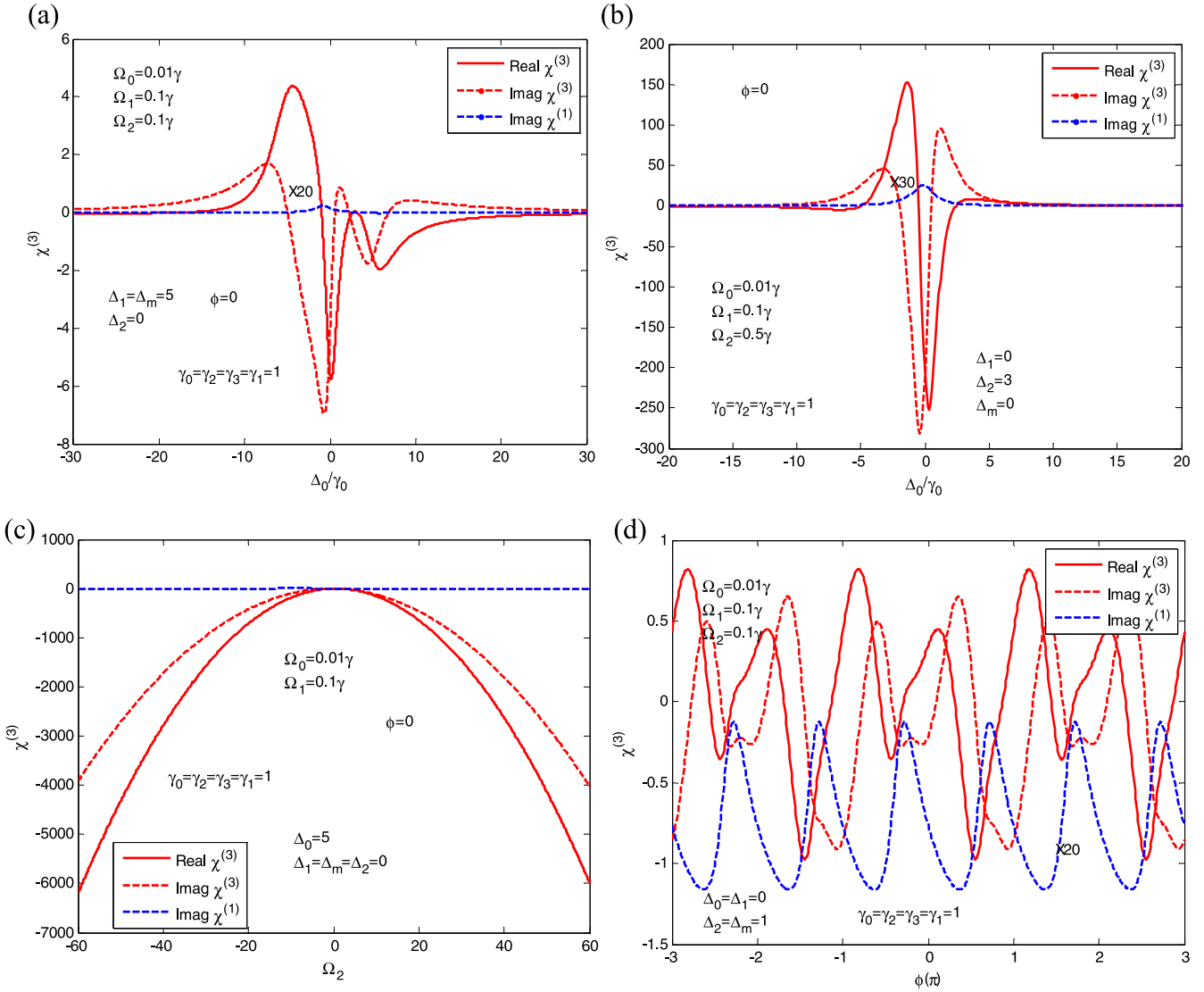


**Figure 6.** Third-order susceptibility for staircase-configuration ( $E_m = 0$ ) when (a) ( $\Omega_0 = 0.01\gamma$ ,  $\Omega_1 = 0.1\gamma$ ,  $\Omega_2 = 0.1\gamma$ ), ( $\Delta_1 = \Delta_m = 5\gamma$ ,  $\Delta_2 = 0$ ); (b) ( $\Omega_0 = 0.01\gamma$ ,  $\Omega_1 = 0.1\gamma$ ,  $\Omega_2 = 0.5\gamma$ ) and ( $\Delta_1 = \Delta_m = 0$ ,  $\Delta_2 = 3\gamma$ ) as a function of probe detuning, ( $\Delta_0$ ), normalized to the decay rate ( $\gamma_0$ ); (c) as a function of coupling field Rabi energy  $\Omega_2$  when ( $\Omega_0 = 0.01\gamma$ ,  $\Omega_1 = 0.1\gamma$ ) ( $\Delta_0 = 5\gamma$ ,  $\Delta_1 = \Delta_2 = \Delta_m = 0$ ); in (d) as a function of phase when ( $\Omega_0 = 0.01\gamma$ ,  $\Omega_1 = 0.1\gamma$ ,  $\Omega_2 = 0.1\gamma$ ), and ( $\Delta_0 = \Delta_1 = 0$ ,  $\Delta_2 = \Delta_m = 1\gamma$ ). Note that ( $\gamma_0 = \gamma_1 = \gamma_2 = \gamma_3 = \gamma = 1$  meV).

detunings, the EIT window is increased by  $\sim 3$  times while Kerr height is reduced by  $\sim$ one order of magnitude. This shows the importance of working with resonant fields (zero detunings) in increasing Kerr height. Switching from negative dispersion to positive is also shown here (figure 5(a)). Figure 5(c) shows Kerr dispersion controlling by field strength; the coupling field is used as an example. A giant Kerr is obtained at zero absorption, which corresponds to distortionless propagation, when a high coupling field is used. Figure 5(d) shows the phase controllability of the  $\Lambda$  configuration system where a high dispersion is obtained at neglected absorption.

d. For  $E_m = 0$ , staircase-configuration

$$\rho_{10}^{(3)} = \left[ \frac{1}{(i\Delta_0 + \gamma_0)} \right] \left\{ \frac{-\Omega_0^2}{\gamma_0} \left[ -i\Omega_0 + \frac{\Omega_0\Omega_1\rho_{21}e^{2i\phi}}{a} \right] \right. \\ \left. \cdot \left[ (i\Delta_0 + \gamma_0) + \frac{\Omega_1^2 e^{2i\phi}}{a} \right]^{-1} + \frac{\Omega_0^2}{\gamma_0} \right. \\ \left. \times \left[ i\Omega_0 + \frac{-\Omega_0\Omega_1\rho_{21}e^{-2i\phi}}{a} \right] \right. \\ \left. \times \left[ (i\Delta_0 + \gamma_0) - \frac{\Omega_1^2 e^{-2i\phi}}{a} \right]^{-1} + \frac{-\Omega_1\Omega_0e^{2i\phi}}{a} \right.$$

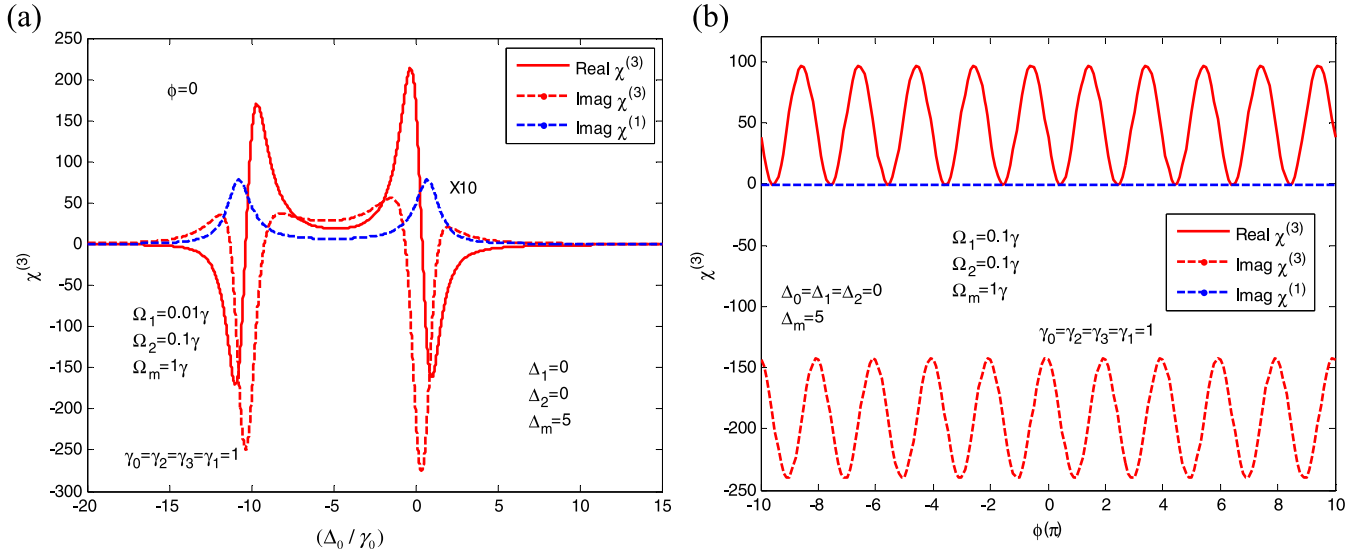


**Figure 7.** Third-order susceptibility for weak probe-configuration ( $E_0 = 0$ ) as a function of probe detuning, normalized to the decay rate ( $\gamma_0$ ) when (a) ( $\Omega_1 = 0.01\gamma$ ,  $\Omega_2 = 0.1\gamma$ ,  $\Omega_m = 1\gamma$ ), ( $\Delta_1 = \Delta_2 = 0$ ,  $\Delta_m = 5\gamma$ ); (b) as a function of phase when ( $\Omega_1 = 0.1\gamma$ ,  $\Omega_2 = 0.1\gamma$ ,  $\Omega_m = 1\gamma$ ) and ( $\Delta_0 = \Delta_1 = \Delta_2 = 0$ ,  $\Delta_m = 5\gamma$ ). Note that ( $\gamma_0 = \gamma_1 = \gamma_2 = \gamma_3 = \gamma = 1$  meV).

$$\begin{aligned} & \times \left[ -i\Omega_0 + \frac{\Omega_0\Omega_1\rho_{21}e^{2i\varphi}}{a} \right] \left[ (i\Delta_0 + \gamma_0) + \frac{\Omega_1^2 e^{2i\varphi}}{a} \right]^{-1} \\ & + \frac{-\Omega_2\Omega_1 e^{i\varphi}}{a} \left[ \frac{i(\Omega_2\rho_{20})}{b} \right] \\ & + \frac{\Omega_0\Omega_1 e^{2i\varphi}}{a} \left[ \frac{-i(\Omega_0\rho_{20}e^{-i\varphi} - \Omega_1)}{[-i\Delta_1 + (\gamma_1 + \gamma_0)]} \right] \end{aligned} \quad (8)$$

Figure 6(a) shows the linear and nonlinear susceptibility when the pump field is turned off and the other parameters are ( $\Delta_1 = \Delta_m = 5\gamma$ ,  $\Delta_2 = 0$ ,  $\Omega_0 = 0.01\gamma$ ,  $\Omega_1 = 0.1\gamma$ ,  $\Omega_2 = 0.1\gamma$ ) where the Kerr dispersion is reduced by three orders of magnitude, compared with figure 5(a), and a negative slope of Kerr dispersion is obtained near zero probe detuning at the neglected absorption (which is multiplied by 20, for figure clarity). Figure 6(b) shows that increasing the coupling field to ( $\Omega_2 = 0.5\gamma$ ) returns the Kerr height to the same range obtained in figure 5(a), which means that the high coupling field works as the main controlling field in the staircase system. A simple two-level behavior is obtained in both figures 6(a) and (b). This may result from the constructive interference between cycling and coupling fields, which removes the EIT window and returns the structure to a simple ( $|1\rangle \rightarrow |0\rangle$ ) system. The benefit of this staircase system compared with any two-level system is the high Kerr value obtained, with negative slope dispersion, at  $\sim$ zero gain. Figure 6(c) shows the case wherein the coupling field is controlled by the system. A high negative Kerr dispersion is obtained at zero absorption. Figure 6(d) shows the phase controllability of this staircase system.

e. For weak probe configuration,  $\Omega_0 = 0$

$$\begin{aligned} \rho_{10}^{(3)} = & \left\{ \frac{-\Omega_2\Omega_1 e^{i\varphi}}{a} \left[ \frac{i(\Omega_m\rho_{10} + \Omega_2\rho_{20})}{b} \right] + \frac{\Omega_m^2}{b} \right. \\ & \times \left[ \frac{\Omega_2\Omega_m\rho_{20}}{b} \right] \left[ (i\Delta_0 + \gamma_0) + \frac{\Omega_1^2 e^{2i\varphi}}{a} + \frac{\Omega_m^2}{b} \right]^{-1} \\ & \left. + \frac{-i(\Omega_2\Omega_m\Omega_1\rho_{10}e^{i\varphi})}{a \cdot b} \right\} \left[ \frac{1}{(i\Delta_0 + \gamma_0)} \right] \end{aligned} \quad (9)$$

Figure 7(a) shows the case when the probe field is turned off. The structure is connected now with the coupling and pump fields. A negative and steep Kerr dispersion is obtained around zero detuning with a considerable nonlinear gain. The EIT window with neglected linear gain peaks (multiplied by 10, for figure clarity) is shown. Figure 7(b) shows the phase control of the weak probe case of our structure. High Kerr peaks are obtained at zero linear gain values.

### 5. Discussion of the cases

Our structure has two branches: the left branch, which is a simple three-level ladder system, and the right branch, which is a staircase- scheme (also equivalent to a ladder system). Inclusion of both Y-branches yields a giant Kerr dispersion as in figure 2; this is also the case when the coupling field is canceled, as in figure 3(b), since both branches are still working. This shows the importance of the case where both branches of Y-structure are coupled by pumping fields (pump, cycling, and controlling fields), compared with the Y-system couples by pump and probe only. Stopping one of

Y-branches returns the structure to a ladder system and reduces its Kerr dispersion comparable to that in [10]. This can be shown for both the left and right branches in figures 4(a) and 6(a), respectively. Kerr dispersion can be increased by using a high value of pump for the ladder-scheme (figure 4(b)) or a high value of coupling field for the staircase-scheme (figure 6(b)).

## 6. Conclusions

A model for the Kerr effect in a Y-configuration in a double quantum dot (QD) system is proposed using the density matrix formalism. Inhomogeneity in QDs is shown to be critical in the dispersion Kerr calculations in QD systems. Five cases are discussed for Y, ladder, staircase,  $\Lambda$ , and weak probe configurations, where the corresponding field is turned off. It is found that in some cases the system returns to a simple two-level state although the Kerr value remains high compared with conventional two-level systems as a result of the collective work of the four fields. Using the controllable fields, detunings and phases, a switching between sub- and superluminal light propagations, distortionless propagation, wide EIT and a giant Kerr nonlinearity is obtained.

## References

- [1] Hamed H R, Asadpour S H and Sahrai M 2013 *Giant Kerr Nonlinearity in a Four-Level Atomic Medium* *Optik* **124** 366–70
- [2] Bai Y, Liub T and Yu X 2013 *Giant Kerr Nonlinearity in an Open V-Type System with Spontaneously Generated Coherence* *Optik* **124** 613–6
- [3] Wang L G, Qamar S, Zhu S Y and Zubairy M S 2008 Manipulation of the raman process via incoherent pump, tunable intensity, and phase control *Phys. Rev. A* **77** 0333833
- [4] Yan D, Liu Y M, Bao Q Q, Fu C B and Wu J H 2012 Electromagnetically induced transparency in an inverted-Y system of interacting cold atoms *Phys. Rev. A* **86** 023828
- [5] Hao X, Yang W X, Lua X, Liu J, Huang P, Ding C and Yang X 2008 Polarization qubit phase gate in a coupled quantum-well nanostructure *Phys. Lett. A* **372** 7081–5
- [6] Asadpour S H, Sahrai M, Sadighi-Bonabi R, Soltani A and Mahrani H 2011 Enhancement of Kerr nonlinearity at long wavelength in a quantum dot nanostructure *Physica E* **43** 1759–62
- [7] She Y, Zheng X, Wang D and Zhang W 2013 Controllable double tunneling induced transparency and solitons formation in a quantum dot molecule *Optics Express* **21** 17392–403
- [8] Mahmoudi M and Sahrai M 2009 Absorption-free superluminal light propagation in a quantum-dot molecule *Physica E* **41** 1772–8
- [9] Hao X, Wu J and Wang Y 2012 Steady-state absorption–dispersion properties and four wave mixing process in a quantum dot nanostructure *J. Opt. Soc. Am. B* **29** 420–8
- [10] Hamed H R, Asadpour S H and Sahrai M 2013 Giant Kerr nonlinearity in a four-level atomic medium *Optik* **124** 366–70
- [11] Joshi A 2009 Phase-dependent electromagnetically induced transparency and its dispersion properties in a four-level quantum well system *Phys. Rev. B* **79** 115315
- [12] Chuang S L 2009 *Physics of Photonic Devices* (New Jersey USA: Wiley)
- [13] Kim J and Chuang S L 2006 Theoretical and experimental study of optical gain, refractive index change, and linewidth enhancement factor of p-doped quantum-dot lasers *IEEE J. Quantum Electron.* **42** 942–52
- [14] Kim J and Chuang S L 2006 Theoretical and experimental study of optical gain, refractive index change, and linewidth enhancement factor of p-doped quantum-dot lasers *IEEE J. Quantum Electron.* **42** 942–52
- [15] Tarasov G G, Zhuchenko Z Y, Lisitsa M P, Mazur Y I, Wang M Z, Salamo G J, Warming T, Bimberg D and Kissel H 2006 Optical detection of asymmetric quantum-dot molecules in double-layer InAs/GaAs structures *Semiconductors* **40** 79–83
- [16] Sahrai M, Tajalli H, Kapale K T and Zubairy M S 2004 Tunable phase control for subluminal to superluminal light propagation *Phys. Rev. A* **70** 023813
- [17] Jiang Y and Zhu K 2008 Controlling Kerr nonlinearity with electric fields in asymmetric double quantum-dots arXiv 0801.3726v1 [cond-mat.mes-hall]
- [18] Mahmoudi M and Sahrai M 2009 Absorption-free superluminal light propagation in a quantum-dot molecule *Physica E* **41** 1772–8
- [19] Al-Khursan A H, Al-Khakani M K and Al-Mossawi K H 2009 Third-order non-linear susceptibility in a three-level QD system *Photonics and Nanostructures-Fundamentals and Applications* **7** 153–60
- [20] Bimberg D, Kirstaedter N, Ledentsov N N, Alferov Z I, Kop'ev P S and Ustinov V M 2000 InGaAs–GaAs quantum-dot lasers *IEEE J. Select. Top. Quantum Electron.* **3** 196–205
- [21] Chang-Hasnain C J and Chuang S L 2006 Slow and fast light in semiconductor quantum-well and quantum-dot devices *J. Lightwave Technology* **24** 4642–54